

The MCXC: a Meta-Catalogue of X-ray detected Clusters of galaxies

R. Piffaretti¹, M. Arnaud¹, G.W. Pratt¹, E. Pointecouteau² and J.-B. Melin³

¹ Laboratoire AIM, IRFU/Service d'Astrophysique - CEA/DSM - CNRS - Université Paris Diderot, Bât. 709, CEA-Saclay, F-91191 Gif-sur-Yvette Cedex, France

² Université de Toulouse, CNRS, CESR, 9av. du colonel Roche, BP 44346, 31028 Toulouse Cedex 04, France

³ DSM/Irfu/SPP, CEA/Saclay, F-91191 Gif-sur-Yvette Cedex, France

Received ; accepted

ABSTRACT

We present the compilation and properties of a Meta-Catalogue of X-ray detected Clusters of galaxies, the MCXC. This very large catalogue is based on publicly available ROSAT All Sky Survey-based (NORAS, REFLEX, BCS, SGP, NEP, MACS, and CIZA) and serendipitous (160SD, 400SD, SHARC, WARPS, and EMSS) cluster catalogues. Data have been systematically homogenised to an overdensity of 500, and duplicate entries originating from overlaps between the survey areas of the individual input catalogues are carefully handled. The MCXC comprises 1743 clusters with virtually no duplicate entries. For each cluster the MCXC provides: three identifiers, a redshift, coordinates, membership of original catalogue, and standardised 0.1 – 2.4 keV band luminosity L_{500} , total mass M_{500} , and radius R_{500} . The meta-catalogue additionally furnishes information on overlaps between the input catalogues and the luminosity ratios when measurements from different surveys are available, and also gives notes on individual objects. The MCXC is available in electronic format for maximum usefulness in X-ray, SZ, and multi-wavelength studies.

Key words. Catalogs, Cosmology: observations, Cosmology: large-scale structure of Universe, Galaxies: cluster: general - X-rays: galaxies: clusters

1. Introduction

Clusters of galaxies provide cosmological constraints through the number density and evolution of objects, through the power spectrum of their three-dimensional distribution, and through their baryon fraction and its evolution. Moreover, the physical properties of clusters provide a test of the structure formation scenario, giving vital information both for understanding the gravitational collapse of the dark matter and for the evolution of baryons in the dark matter potential (see Voit 2005, for a review).

X-ray observations are ideal for these studies as the density squared dependence of the X-ray emission means that clusters can efficiently be found over a wide redshift range. Cluster sources were evident in the first all-sky X-ray survey with *Uhuru*, and further objects were found by HEAO-1 and *Ariel-V*; subsequent follow-up observations with *Einstein* and *EXOSAT* allowed more accurate characterisation of their physical properties (see Rosati et al. 2002, for a review).

In this context, the ROSAT satellite has played a central role. The 1990-1991 ROSAT All-Sky Survey (RASS, Voges et al. 1999) and later deep pointed observations have led to the discovery of hundreds of clusters. Subsequent follow-up observations, in particular those conducted with the current generation of X-ray satellites *XMM-Newton*, *Chandra* and *Suzaku*, have provided statistical samples for cosmological studies (e.g., Vikhlinin et al. 2009; Mantz et al. 2009) and detailed information on the structural properties of the cluster population (e.g., Vikhlinin et al. 2006; Pratt et al. 2010; Arnaud et al. 2010). Other observations have allowed in-depth study of the hierarchical assembly process

through merging (e.g., Markevitch & Vikhlinin 2007) and the physical mechanisms associated with feedback and its impact on structure formation (e.g., McNamara & Nulsen 2007, and references therein). However, while several *XMM-Newton* and *Chandra* X-ray surveys are ongoing (e.g., Romer et al. 2001; Barkhouse et al. 2006; Pacaud et al. 2007; Fassbender 2007)¹, the associated cluster catalogues are either not yet published or only partially available.

Outside of the X-ray domain, the redshift-independent thermal Sunyaev-Zel'dovich effect (Sunyaev & Zel'dovich 1972, hereafter SZ) is emerging as an efficient way to detect distant, massive clusters that fall below the flux limits of X-ray surveys. Several SZ surveys, including the South Pole Telescope (SPT, Carlstrom et al. 2009) survey, the Atacama Cosmology Telescope (ACT, Fowler et al. 2007), and Planck (Tauber et al. 2010), are actively ongoing and have started providing the first SZ-selected cluster catalogues (e.g., Vanderlinde et al. 2010; Menanteau et al. 2010). X-ray observations of SZ clusters are important in many respects. The X-ray properties allow a better characterisation of the SZ signal (e.g., Melin et al. 2006; Andersson et al. 2010) and yield the calibration of the scaling relations needed for cosmological studies with SZ-selected cluster samples (e.g., Majumdar & Mohr 2003). In addition, X-ray observations allow testing of the selection function of SZ surveys and verification of new SZ cluster candidates (e.g., Šuhada et al. 2010). Moreover, they are essential for statistical analyses of the SZ data (e.g., Melin et al. 2010; Komatsu et al. 2010, and references therein).

Send offprint requests to: R. Piffaretti, e-mail: rocco.piffaretti@cea.fr

¹ See <http://cxc.harvard.edu/xraysurveys/surveys.html> for a complete list of ongoing *XMM-Newton* and *Chandra* surveys.

Cosmological tests that rely on knowledge of the evolution of the mass function or baryon fraction require an estimate of the cluster mass. Surveys provide only an observable (typically luminosity, temperature or SZ y -parameter) that is then linked to the cluster mass via scaling relations. While simultaneous constraints on cosmological parameters and scaling relations have recently been derived (Mantz et al. 2009), the mass proxy relations are typically separately calibrated using deep observations of well-understood and if possible representative samples (e.g., Arnaud et al. 2007; Maughan 2007; Vikhlinin et al. 2009; Pratt et al. 2009). Although their redshift evolution is at present poorly known, a consensus on the type of scaling relations to be calibrated and their precise definition has been reached. For example, the bias introduced by cool core clusters in luminosity and temperature measurements is taken into account, low scatter mass proxies such as Y_X (Kravtsov et al. 2006) or the gas mass M_{gas} are widely used, and all quantities are measured up to a standard characteristic radius R_{500} , the radius within which the mean over-density of the cluster is 500 times the critical density at the clusters redshift. Substantial progress has also been made in understanding the systematics affecting X-ray mass estimates via simulations (e.g., Rasia et al. 2006; Nagai et al. 2007a; Piffaretti & Valdarnini 2008) and via combination with gravitational lensing (e.g., Mahdavi et al. 2008; Zhang et al. 2010; Meneghetti et al. 2010).

ROSAT-derived catalogues still play a major role in providing targets for deeper observation with the current generation of X-ray instruments (e.g., Böhringer et al. 2007; Vikhlinin et al. 2009), and for identification of existing clusters in new surveys in other wavelength bands (e.g., Popesso et al. 2004). These catalogues have been derived from a number of surveys based on RASS data or ROSAT pointed observations (see Sect. 2). Despite the fact that these catalogues are public, no attempt has yet been made to merge them and to homogenise the data contained within. The main reasons for this are their large sizes and the fact that different catalogues provide different types of information.

Given the current status of X-ray cluster catalogues, and the relevance of scaling relations for SZ surveys and X-ray studies in general, we collected data from all the major public X-ray survey catalogues and homogenised the information to provide the community with a meta-catalogue of X-ray detected clusters of galaxies (hereafter the MCXC). The basic characteristics of the MCXC are the large number of clusters in the catalogue (1743 unique systems), a uniform format for all provided quantities, careful control of duplicate entries originating from overlaps between the input catalogues, and homogeneously estimated 0.1 – 2.4 keV band luminosities L_{500} and total masses M_{500} . In order to be easily manipulated, the MCXC is provided in electronic format. The final catalogue gives a first overview of the published, publicly-available X-ray survey selected cluster population.

The paper is organised as follows. In Sect. 2 we describe the basic properties of the catalogues used to construct the MCXC. In Sect. 3 we explain how the information is homogenised and detail the quantities provided by the MCXC. The handling of duplicate entries is presented in Sect. 4 and in Sect. 5 we discuss various aspects of the final catalogue. In Sect. 6 we summarize our results and present our conclusions.

As a cosmological model we adopt a Λ CDM cosmology with $H_0 = 70$ km/s/Mpc, $\Omega_M = 0.3$ and $\Omega_\Lambda = 0.7$ throughout the paper. The quantity $h(z)$ is the ratio of the Hubble constant at redshift z to its present value, H_0 , i.e., $h(z)^2 = \Omega_m(1+z)^3 + \Omega_\Lambda$.

2. Input X-ray catalogues

In the following we describe the input catalogues used to construct the MCXC. We recall the basic characteristics of the X-ray surveys used to construct each catalogue and how the X-ray quantities adopted in our work are measured. We discuss only X-ray information essential to the MCXC and focus on the quantities that allow us to compute the luminosities, L_{500} . For more details on the individual surveys, and in particular the associated optical observations/followup, we refer the reader to the cited papers and references therein.

Generally speaking, two types of X-ray survey can be distinguished: contiguous area surveys, which use data from the ROSAT All-Sky Survey (RASS, Voges et al. 1999), and serendipitous cluster surveys, which are based on data from deeper pointed X-ray observations. In the following, we therefore distinguish between RASS-based and serendipitous catalogues. In addition to handling duplicate entries and removing particular clusters as discussed below, we exclude clusters with non measured redshifts or luminosities. Table 1 summarises the contributions of the various input catalogues to the MCXC.

The bulk of the X-ray data used to construct the MCXC are derived from ROSAT observations. Exceptions are EMSS and some physical quantities for MACS, as described in more detail below. Future work will include as-yet unpublished catalogues such as RDCS (the ROSAT Deep Cluster Survey, Rosati et al. 1998), XCS (the XMM Cluster Survey, Romer et al. 2001), XDCCP (the XMM-Newton Distant Cluster Project, Fassbender 2007), and the complete MACS catalogue (Ebeling et al. 2001).

2.1. RASS-based catalogues

We compiled data from nine RASS-based contiguous area surveys, as described below.

2.1.1. REFLEX and NORAS

REFLEX (ROSAT-ESO Flux Limited X-ray Galaxy Cluster Survey, Böhringer et al. 2004a) is based on RASS data for a survey area covering the southern sky up to a declination $\delta = 2.5$ deg with the galactic plane ($|b| \leq 20$ deg) and the regions of the Magellanic clouds excluded. The total survey area is 13924 deg² and the survey is flux-limited (0.1 – 2.4 keV band flux $\geq 3 \times 10^{-12}$ erg s⁻¹ cm⁻²).

NORAS (Northern ROSAT All-Sky galaxy cluster survey Böhringer et al. 2000a) is also based on RASS data excluding the same region around the galactic plane, but covers the northern sky. This survey catalogue is not flux-limited and selection is based on minimum count rate (0.06 cts/s in the 0.1 – 2.4 keV band) and a source extent likelihood.

The data analysis and catalogue production for both NORAS and REFLEX are performed by essentially the same authors and, although REFLEX has been more extensively studied and characterised than NORAS, the information provided is extremely similar. A growth curve analysis is adopted to determine source fluxes (the typical flux measurement accuracy is 10 – 20%) and luminosities. The REFLEX catalogue provides aperture luminosities L_{ap} as well as total luminosities. The latter are computed by estimating the missing flux outside the detection aperture by assuming a β -model with $\beta = 2/3$, a core radius r_c which scales with mass, and a cluster extent of $12 \times r_c$. For the NORAS clusters a similar procedure is performed, but the resulting total luminosities are not reported. Therefore the NORAS catalogue provides only aperture luminosities.

For both catalogues data (Böhringer et al. 2000b, 2004b) are retrieved from Vizier². Because of the homogeneity of these two catalogues we merge them into a single NORAS/REFLEX catalogue. The names NORAS and REFLEX are kept as sub-catalogue labels. Because of the overlap of the NORAS and REFLEX survey areas, there are ten duplicate entries. For these ten clusters the information provided by NORAS and REFLEX is almost identical and we exclude, for each of the duplicates, the cluster with the larger flux uncertainty.

Since the number of clusters in the combined NORAS/REFLEX catalogue is large (889 objects, see Table 1) and because the information provided by the authors is homogeneous and detailed, it is the cornerstone of the MCXC.

2.1.2. ROSAT BCS and eBCS

The **ROSAT BCS** (The ROSAT Brightest Cluster Sample, Ebeling et al. 1998) comprises the brighter sources of the NORAS survey. We use data for the 90 per cent complete BCS, a flux-limited sample ($0.1 - 2.4$ keV band flux $\geq 4.4 \times 10^{-12}$ erg s⁻¹ cm⁻²) of $z \leq 0.3$ clusters.

The **eBCS** (The extended ROSAT Brightest Cluster Sample, Ebeling et al. 2000a) is the low flux extension of the BCS ($0.1 - 2.4$ keV band flux $\geq 2.8 \times 10^{-12}$ erg s⁻¹ cm⁻²).

The type of information provided is the same for both samples. In both cases detection and cluster emission characterisation are based upon the Voronoi tessellation and percolation (VTP) algorithm. The emission outside the detection region is computed by correcting the detected count rate. For clusters this is undertaken by assuming a β -model profile with $\beta = 2/3$ and a core radius estimated from the source profile, taking into account the telescope PSF. The resulting total luminosities, the corrected and uncorrected count rates, and the VTP aperture radius are provided. This implies that the luminosity within the VTP aperture radius can be computed for all the clusters in the sample.

Data (Ebeling et al. 2000b,c) are retrieved from Vizier and merged into a single BCS catalogue where the names BCS and eBCS are kept as sub-catalogue labels (see Table 1). Note that there is only one cluster, A1758a, that is listed in both BCS and eBCS. The two luminosities are almost identical and we remove it from the BCS sub-catalogue. In addition, for the Virgo cluster we adopt the luminosity estimate of Böhringer et al. (1994).

2.1.3. SGP

The **SGP** (A Catalog of Clusters of Galaxies in a Region of 1 Steradian around the South Galactic Pole, Cruddace et al. 2002a) covers a region of 1.013 sr centered on the south Galactic pole and is based on the same X-ray source detection and characterisation procedures as REFLEX. The lowest detected flux is 1.5×10^{-12} erg s⁻¹ cm⁻² in the $0.1 - 2.4$ keV band, and a complete sub-sample can be obtained by imposing a flux limit of 3×10^{-12} erg s⁻¹ cm⁻².

Luminosities are computed within a cutoff radius provided by the growth curve analysis. Since the cutoff radius is not given in the catalogue, we treat the quoted luminosity as the total luminosity.

Data for the entire non-flux-limited, SGP sample (Cruddace et al. 2002b, 2003) were retrieved from Vizier.

2.1.4. NEP

The **NEP** (The ROSAT North Ecliptic Pole survey, Henry et al. 2006) surrounds the north ecliptic pole in a survey area of 80.6 deg², and has the deepest exposure in the northern RASS (exposure times from 2000 to over 40000 s). Source detection is based on Voges et al. (1999) and the selection is performed by adopting thresholds for the source extent likelihood and signal-to-noise ratio.

The quoted total luminosities are computed from size corrected fluxes. The latter are computed from detected fluxes within apertures of radius $5'$ ($6.5'$ for RXJ1834.1+7057) by assuming a PSF-corrected β -profile with $\beta = 2/3$ and a fixed core radius of 180 kpc. The profile is integrated up to R_{200} , which is estimated from the size-temperature relation of Evrard et al. (1996). Size correction factors are provided so that aperture luminosities can be computed.

Data for the whole flux-limited sample ($0.5 - 2$ keV band flux $\geq 2. \times 10^{-14}$ erg s⁻¹ cm⁻², Henry et al. 2006) were retrieved from Vizier, and only sources identified as clusters were selected (see Table 1).

2.1.5. MACS

The **MACS** (Massive Cluster Survey, Ebeling et al. 2001) is based on the ROSAT Bright Source Catalogue with the aim of increasing the number of known very luminous, $z \geq 0.3$ clusters. A MACS catalogue has not yet been published in its entirety and we therefore collected data from different publications as detailed below. Notice that the data reported in these publications are based on *Chandra* follow-up observations and that these publications yield all publicly-available MACS clusters with coordinates, redshifts, and luminosities (i.e., the minimal set of quantities required for the MCXC).

Properties of a complete subsample of $z > 0.5$ MACS clusters (the MACS_DIST sub-catalogue, twelve objects) are listed in Ebeling et al. (2007). A further complete subsample of bright objects in the $0.3 < z < 0.5$ redshift range (the MACS_BRIGHT sub-catalogue, 34 clusters) are given in Ebeling et al. (2010). For these sources, the luminosities within R_{200} are listed. For 32 of the 34 MACS_BRIGHT clusters Mantz et al. (2009) give additional properties such as L_{500} , M_{500} , etc³. This information is also merged into the MACS_BRIGHT sub-catalogue.

Further MACS clusters are analysed in Maughan et al. (2008, the MACS_MJFV sub-catalogue, 23 objects), who provide very complete information on the physical properties of these objects. Of the MACS_MJFV sample there are six clusters in common with the MACS_DIST sub-catalogue and twelve clusters in common with the MACS_BRIGHT sub-catalogue. We construct a unique MACS catalogue by merging the three sub-catalogues and keeping only measurements given by Maughan et al. (2008) for the eighteen duplicate clusters (see Table 1). Apart from the six MACS_DIST luminosity measurements in Ebeling et al. (2007), the luminosities L_{500} are directly available for all MACS clusters.

2.1.6. CIZA

The **CIZA** (Clusters in the Zone of Avoidance, Ebeling et al. 2002 and Kocevski et al. 2007, respectively **CIZAI** and **CIZAII**) catalogues are based on the ROSAT Bright Source

² <http://VizieR.u-strasbg.fr/viz-bin/VizieR>

³ MACSJ0358.8-2955 and MACSJ2311.5+0338 are not studied in Mantz et al. (2009).

Catalogue and focus on the region around the galactic plane ($|b| \leq 20$ deg). Candidate selection is based on limits on the detected fluxes and spectral hardness ratios. CIZAI comprises the X-ray brightest objects ($\text{flux} \geq 5. \times 10^{-12} \text{ erg s}^{-1} \text{ cm}^{-2}$), while CIZAII is its low-flux extension ($\text{flux} \geq 3. \times 10^{-12} \text{ erg s}^{-1} \text{ cm}^{-2}$).

Quoted luminosities are computed from raw RASS data using very large apertures and can be therefore safely interpreted as total luminosities.

The type of data available for the two catalogues is identical, and after retrieving data (Ebeling et al. 2002; Kocevski et al. 2007) from Vizier, we merged them into a single CIZA catalogue where the names CIZAI and CIZAII define the sub-catalogues (see Table 1).

2.2. Serendipitous catalogues

We compiled data from a further seven serendipitous surveys as described below.

2.2.1. 160SD

The **160SD** (The 160 Square Degree ROSAT Survey, Mullis et al. 2003) is based on the serendipitous detection of extended X-ray emission in 647 archival ROSAT PSPC observations. With the galactic plane ($|b| \leq 30$ deg) and the regions of the Magellanic clouds excluded, the resulting sky coverage at high fluxes is 160 deg^2 .

A wavelet algorithm is used to detect galaxy clusters and the quoted total luminosities are computed from the detected fluxes by assuming a β -profile with $\beta = 2/3$ and a fitted core radius.

We retrieved the full dataset (Mullis et al. 2003) from Vizier and selected only sources identified as galaxy clusters.

2.2.2. 400SD

The **400SD** (The 400 Square Degree ROSAT PSPC Galaxy Cluster Survey, Burenin et al. 2007) extends the 160SD methodology to additional PSPC observations by adopting less restrictive selection criteria (e.g., galactic latitude and absorption, exposure times). A total of 1610 fields, corresponding to a total survey area of 397 deg^2 , are analysed to yield a large flux-limited ($0.5 - 2 \text{ keV}$ band flux $\geq 1.4 \times 10^{-13} \text{ erg s}^{-1} \text{ cm}^{-2}$) cluster catalogue. 400SD data is available for serendipitously and not entirely serendipitously detected clusters (clusters at redshift very close to the target redshift).

We retrieved data (Burenin et al. 2009) from Vizier, and merged the information into a unique 400SD catalogue, introducing the sub-catalogue labels **400SD_SER** and **400SD_NONSER** to distinguish between the two classes of objects (see Table 1).

2.2.3. SHARC Bright and SHARC Southern

The SHARC survey is based on archival ROSAT PSPC observations. The **SHARC Bright** (Bright Serendipitous High-Redshift Archival ROSAT Cluster survey, Romer et al. 2000a) is a wide area shallow survey covering a total area of 178.6 deg^2 with a flux limit of $1.63 \times 10^{-13} \text{ erg s}^{-1} \text{ cm}^{-2}$. The **SHARC Southern** (The Southern Serendipitous High-Redshift Archival ROSAT Cluster survey, Burke et al. 2003a) is a narrow area deep survey covering 17.7 deg^2 with a flux limit of $4.66 \times 10^{-14} \text{ erg s}^{-1} \text{ cm}^{-2}$. Cluster detection is based on a wavelet and sliding-box techniques, respectively.

Table 1. Number of clusters in the catalogues used to construct the MCXC before and after handling of multiple entries.

Catalogue	Nr. of clusters	Nr. of clusters
Sub-catalogues	Input	MCXC
NORAS/REFLEX	889	879
NORAS	445	437
REFLEX	444	442
400SD	266	256
400SD_SER	242	236
400SD_NONSER	24	20
160SD	199	90
BCS	312	80
BCS	205	47
eBCS	107	33
SGP	157	55
SHARC	69	30
SHARC_SOUTH	37	14
SHARC_BRIGHT	32	16
WARPS	159	78
WARPS	34	11
WARPSII	125	67
NEP	63	48
MACS	51	38
MACS_MJFV	23	18
MACS_BRIGHT	22	14
MACS_DIST	6	6
CIZA	130	128
CIZAI	73	72
CIZAII	57	56
EMSS	102	61
EMSS_1994	81	47
EMSS_2004	21	14
TOTAL	2397	1743

For both catalogues a β -profile with fixed $\beta = 2/3$ and r_c is used to determine the total luminosity and a circular aperture of radius r_{80} , which contains 80 percent of the total flux. This implies that in addition to the extrapolated total luminosities, the aperture luminosities $L_{ap} \equiv L(< r_{80})$ are available.

Data (Burke et al. 2003b; Romer et al. 2000b) are retrieved from Vizier and merged into a single SHARC catalogue (only sources identified as clusters are selected from Romer et al. (2000b)) with sub-catalogues labelled SHARC_SOUTH and SHARC_BRIGHT (see Table 1).

2.2.4. WARPS and WARPSII

The WARPS survey is also based on ROSAT PSPC observations. **WARPS** (Wide Angle ROSAT Pointed Survey, Perlman et al. 2002a), covers 16.2 deg^2 in 86 PSPC fields, while its extension **WARPSII** (Wide Angle ROSAT Pointed Survey II, Horner et al. 2008) covers 56.7 deg^2 in 301 PSPC fields. The WARPS survey

uses the VTP algorithm for cluster detection and characterization.

The quoted total luminosities are computed as in Ebeling et al. (1998), but no information which allows the computation of aperture luminosities is reported.

Data (Perlman et al. 2002b; Horner et al. 2009) are retrieved from Vizier. For both catalogues we include clusters below the nominal flux limit that defines the statistically complete sample. The two catalogues are merged into a single WARPS catalogue and WARPSI and WARPSII are adopted as sub-catalogue labels (see Table 1).

2.2.5. EMSS

The **EMSS** (Einstein Observatory Extended Medium Sensitivity Survey, Gioia et al. 1990) cluster catalogue is constructed from a flux-limited sample of sources serendipitously detected in *Einstein* IPC (Imaging Proportional Counter) fields at high galactic latitudes.

Data are compiled from the tables published in Gioia & Luppino (1994) and Henry (2004). While the sample presented in Gioia & Luppino (1994) is the most complete and up-to-date work on the entire EMSS cluster catalogue, Henry (2004) provides more reliable ASCA measurements for the $z \geq 0.3$ EMSS clusters. The *Einstein* luminosities reported in Gioia & Luppino (1994) are computed from the flux measured in a $2'4 \times 2'4$ detection cell by adopting a β -model with fixed $\beta = 2/3$. The information provided is not sufficient to compute aperture luminosities from the quoted total luminosities. The ASCA luminosities in Henry (2004) are total luminosities. Since distant clusters are not resolved by ASCA, these luminosities were derived by assuming that the clusters are point sources. Hence in this case only total luminosities are available.

Clusters in the Henry (2004) sample are removed from Gioia & Luppino (1994)⁴. We remove MS1209.0+3917, MS1333.3+1725, and MS1610.4+6616 for the reasons mentioned in Henry (2004). The data are then merged into a single EMSS catalogue where the names EMSS_1994 and EMSS_2004 denote the sub-catalogue labels (see Table 1).

3. Data extraction and homogenisation

The data provided by the different input catalogues (positions, redshifts, names, luminosities, etc.) are rather similar. However some data homogenisation is needed, in particular for quantities such as luminosity and mass.

As detailed above, in many cases the luminosity is measured within some small aperture R_{ap} ($L_{\text{ap}} \equiv L(< R_{\text{ap}})$) is the corresponding aperture luminosity) and then extrapolated to some larger radius using a reasonable model of the surface brightness profile. The radial extrapolation might be extremely large, implying that the derived luminosity is basically equal to the total luminosity $L_{\text{tot}} = L(< \infty)$. Another common choice is to extrapolate to R_{200} . In this case the luminosity $L_{200} \equiv L(< R_{200})$ is essentially equal to L_{tot} , since the contribution to the total luminosity of the emission between R_{200} and infinity is fully negligible. With the present generation of X-ray observations, the standard choice is R_{500} ($L_{500} \equiv L(< R_{500})$), and we have chosen this radius for the MCXC data homogenisation procedure.

The assumed cosmological model is of course at the basis of our homogenisation procedure. In the following all luminosities

and other cluster parameters which depend on the distance scale are converted to our reference cosmology (i.e. $\Omega_M = 0.3$, $\Omega_\Lambda = 0.7$, and $H_0 = 70$ km/s/Mpc).

Below we list all the quantities that are provided by the MCXC and explain in detail how they are derived from the original information in the input catalogues. The names of the quantities as given in the associated electronic table are given in typewriter typeface. MCXC clusters are ordered by right ascension. As an example we list the first 40 entries by splitting the information into Tables 2 and 3.

3.1. Coordinates and redshifts

The cluster coordinates given in the input catalogues are those of the cluster centroid determined from X-ray data (apart from those in the sub-catalogue EMSS_1994 which are the coordinates of the cluster optical position). For the MCXC, all coordinates are converted to right ascension and declination for the epoch J2000 in hours (degrees), minutes, and seconds (RAJ2000 and DEJ2000) and in units of decimal degrees (_RAJ2000 and _DEJ2000). We also provide the cluster positions in galactic coordinates – GLON and GLAT are galactic longitude and latitude, respectively, in degrees (see Table 2).

No manipulation is needed for the cluster redshifts z . As stated above, only clusters with measured redshift are retained in the MCXC (see Table 2). In Fig. 1, we show the redshift histograms of the individual input catalogues used to construct the MCXC and of the MCXC after handling of multiple entries (see Sect. 4). The histograms highlight the different redshift ranges typically probed by serendipitous and RASS-based surveys, with the latter generally being confined to local and medium redshift clusters.

3.2. Names

Two types of cluster name are usually listed in the input catalogues: the name assigned by the authors **NAME**, and the alternative name **NAME_ALT** (see Table 2). **NAME** is usually constructed from the cluster coordinates (e.g., RXJ0041.1-2339 in 160SD, MS0007.2-3532 in EMSS, MACSJ0011.7-1523 in MACS, RXCJ0000.1+0816 in NORAS/REFLEX, CIZA, and SGP, RXJ1716.6+6410 in NEP and SHARC, J0022.0+0422 in WARPS). Exceptions to this format are BCS and 400SD. BCS names are listed as they appear in optical catalogues (e.g. ZwCl1432, A602), while in the 400SD, names are not assigned. We therefore assigned a **NAME** to 400SD_SER clusters according to the standard SIMBAD⁵ format acronym 'BVH2007 NNN' (Burenin+Vikhlinin+Hornstrup+, 2007, e.g., BVH2007 193), and for the 400SD_NONSER we created a new acronym 'BVH2007 NS NNN' (e.g., BVH2007 NS 12). For all but the 400SD clusters we retain the original names as listed in the input catalogues.

Alternative names in the input catalogues are mostly based on cataloged optical counterparts to the X-ray sources (e.g. A2894, ZwCl 0104.9+5350, UGC 12890). In some cases alternative names are given as notes or comments, and we also use this information to construct **NAME_ALT** in the MCXC by extracting the suitable piece of information. Alternative names are homogenised so as to match both SIMBAD and NED⁶ standards. When this is not possible we choose the SIMBAD acronym conventions. Moreover, when multiple alternative names are avail-

⁴ For a comparison between EMSS and ASCA flux measurements see Henry (2004).

⁵ <http://simbad.u-strasbg.fr/simbad/>

⁶ <http://nedwww.ipac.caltech.edu/>

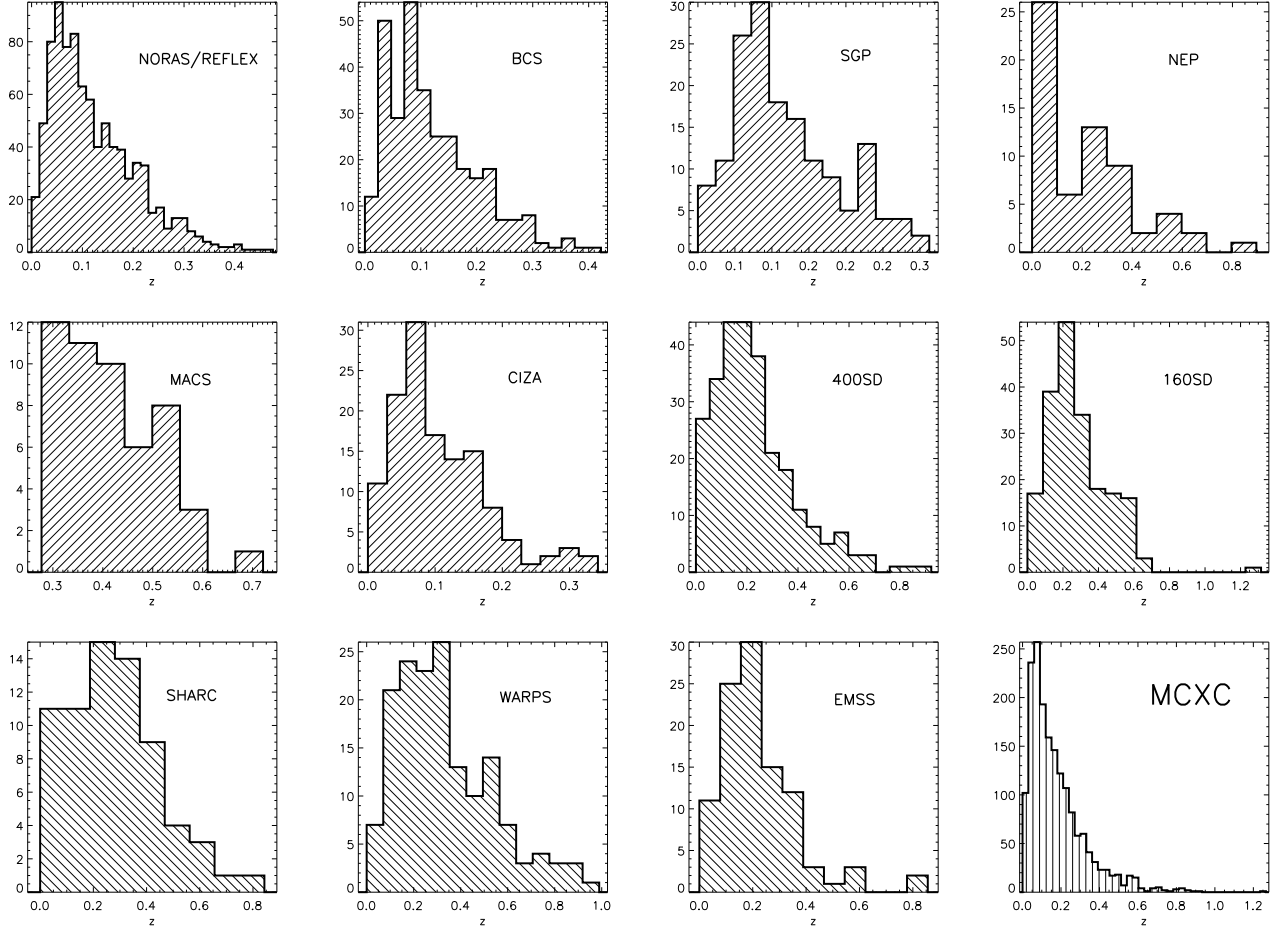


Fig. 1. Redshift histograms of the input catalogues used to construct the MCXC and of the MCXC after handling of multiple entries. Different area shadings are used for RASS-based, serendipitous, and MCXC catalogues.

able, they are listed separated with a comma. For BCS clusters we set `NAME_ALT` equal to `NAME`. For 160SD and 400SD clusters alternative names are extracted from the notes. For 160SD clusters the identifier 'VMF98 NNN' is also used.

Notice that in most of the input catalogues alternative names end with letters for double systems (e.g., A2384 (A), A3574E, etc.). Such information is important because it indicates whether the measured luminosity refers to the whole system to only a part of it.

Our choice of formats for `NAME` and `NAME_ALT` in the MCXC is made in order to facilitate queries in the SIMBAD and NED databases. Notice that both `NAME` and `NAME_ALT` also facilitate the handling of duplicate entries as discussed extensively below in Sect. 4.

In addition to the above two cluster identifiers we add a third name, `NAME_MCXC` (see Table 2), that is constructed from coordinates for the epoch J2000. It allows a fully unambiguous cluster identification in the MCXC catalogue and is defined as `MCXC JHHMM.m+DDMM`.

3.3. Catalogue and Sub-catalogue

As explained above in Sect. 2 and listed in Table 1, for each cluster the input catalogue and sub-catalogue names are given in `CATALOGUE` and `SUB_CATALOGUE` (see Table 2). If no sub-

catalogue exists the sub-catalogue name is equal to the catalogue name.

3.4. Luminosities

The luminosities are homogenised according to the following procedure:

1. When necessary, we first convert the input luminosity (e.g., 0.5 – 2 keV band in NEP, bolometric in MACS_MJFV, 0.3 – 3.5 keV band in EMSS_1994) to the 0.1 – 2.4 keV energy band using the MEKAL plasma code (Mewe et al. 1985; Liedahl et al. 1995). The temperature dependence of this conversion is taken into account by either using measured temperatures when available in the input catalogue, or by iteration about the the non-core-excised luminosity-temperature relation of Pratt et al. (2009), assuming an abundance of 0.3. In the following all the quoted luminosities are therefore as measured in the 0.1 – 2.4 keV energy band for our reference cosmology.
2. The resulting luminosities are then converted to L_{500} adopting two different procedures, depending on the type of luminosity measurement available in the input catalogue.
 - If only the total luminosity L_{tot} (i.e., extrapolated up to large distances) is available we adopt $L_{500} = a \times L_{\text{tot}}$, where a is the ratio L_{500}/L_{tot} for a luminosity profile model based in the average gas density profile derived

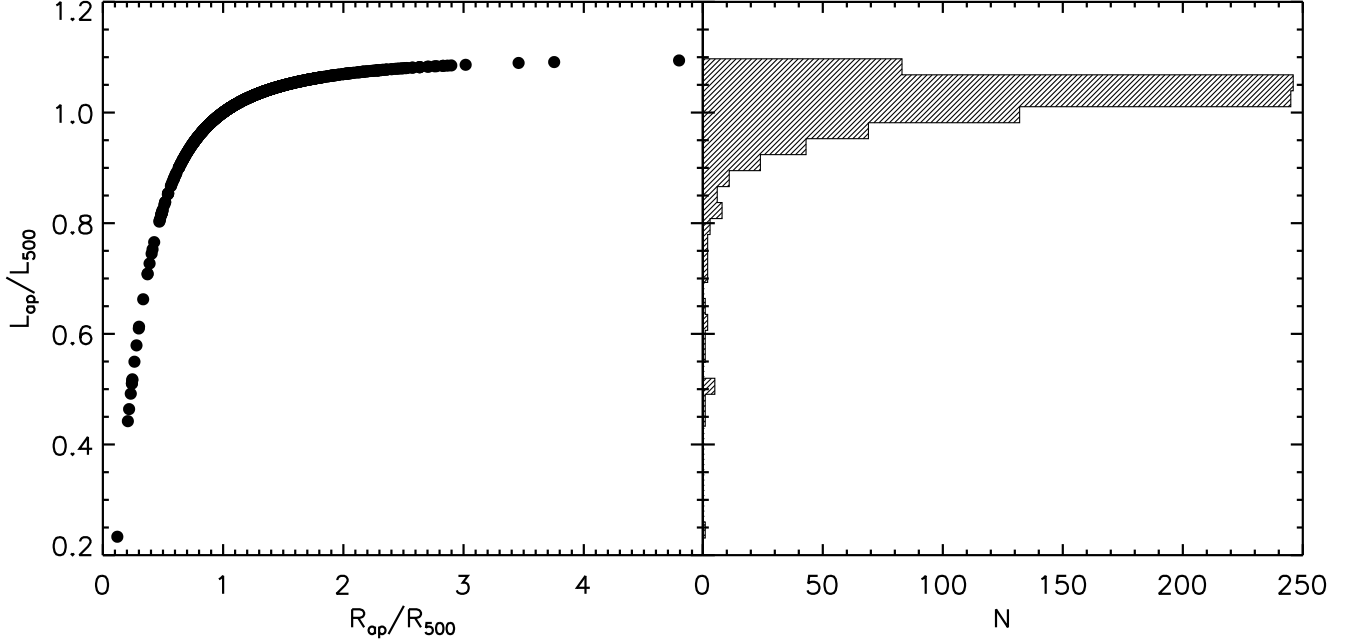


Fig. 2. Relation between input quantities R_{ap} and $L_{ap} = L(< R_{ap})$ and the iteratively estimated R_{500} and $L_{500} = L(< R_{500})$ for the NORAS/REFLEX clusters. The luminosity ratio as a function of aperture radius ratio is shown in the left panel, while the luminosity ratio histogram is shown in the right panel.

from the representative X-ray cluster sample REXCESS (Croston et al. 2008). More precisely, from the individual scaled density profiles (see Arnaud et al. 2010, left panel of Figure 3), we computed the average profile and fitted it with the AB-model given by Eqn. 2 in Pratt & Arnaud (2002):

$$\rho_{gas} \propto \left(\frac{x}{x_c}\right)^{-\alpha} \times \left[1 + \left(\frac{x}{x_c}\right)^2\right]^{-3\beta/2 + \alpha/2}, \quad (1)$$

for $x = r/R_{500}$, finding $x_c = 0.303$, $\alpha = 0.525$, and $\beta = 0.768$.

Since only recently observational progress has shown that the AB-model (Eq. 1) yields a more accurate description than the traditional β -model (see Croston et al. 2008, and references therein), most of the analyses listed in Sect. 2 adopted the latter when extrapolating luminosities to large radii. For the sake of clarity, in Appendix A we illustrate the differences between luminosities computed adopting the AB-model or the β -model.

Since observed luminosities are derived from surface brightness profiles and integration within circular apertures, the resulting luminosity profile is cylindrically integrated up to aperture radii of 1 and $5 \times R_{500}$ to compute L_{500} and L_{tot} , respectively. The cluster boundary is also assumed to be equal to $5 \times R_{500}$. We find a ratio $a = L_{500}/L_{tot} = 0.91$ and that the exact choice of the aperture enclosing the total luminosity is not relevant. This constant $\sim 10\%$ correction is therefore applied to all the 160SD, 400SD, SGP, WARPS, CIZA, MACS_DIST, and EMSS clusters for which only total luminosities are available (see Sect. 2). For the MACS_MJFV and MACS_BRIGHT clusters no conversion is needed since the quoted luminosities are L_{500} .

- For the remaining clusters, i.e. those with available aperture luminosities L_{ap} (1333 objects in total), we compute L_{500} iteratively. The basic ingredients of this iterative procedure are the luminosity profile model implied by Eq. 1 and the luminosity-mass relation (L-M relation, hereafter):

$$h(z)^{-7/3} \left(\frac{L_{500}}{10^{44} \text{ erg s}^{-1}}\right) = C \left(\frac{M_{500}}{3 \times 10^{14} M_{\odot}}\right)^{\alpha}, \quad (2)$$

with $\log(C) = 0.274$ and $\alpha = 1.64$ (see Table 1 in Arnaud et al. 2010). These values are slightly different from those given in Pratt et al. (2009) due to Arnaud et al.’s use of an updated $M_{500} - Y_X$ relation. Specifically, we use the relation in Eq. 2 of Arnaud et al. (2010), i.e. we adopt a non-self-similar slope for the $M_{500} - Y_X$ relation. The adopted C and α values are derived from REXCESS luminosity data uncorrected for the Malmquist bias. The effect of these choices is further discussed below.

In addition to Eqs. 1 and 2, our iterative procedure necessitates the basic input quantities R_{ap} and $L_{ap} = L(< R_{ap})$, the circular aperture radius and the aperture luminosity, respectively. These are either directly available from the input catalogues or can be computed as explained in Sect. 2 for the NORAS/REFLEX, BCS, SHARC, and NEP catalogues.

For each cluster, the aperture luminosity and radius together with the model luminosity profile set the luminosity profile in physical units (i.e. radius in Mpc). The latter are then iteratively converted in units of R_{500} using Eq. 2 by using L_{ap} as the starting luminosity in the iteration. In Fig. 2 we illustrate the relation between the input luminosity L_{ap} and L_{500} for the NORAS/REFLEX clusters. As expected, small/large apertures yield final luminosities L_{500} which are larger/smaller than the input aperture

luminosities (left panel). Notice that while on average the difference between L_{ap} and L_{500} is $\sim 5\%$, it is very relevant for a significant portion of the sample (right panel). In order to explore the effect of our choice of $M_{500} - Y_X$ relation, we iteratively estimate L_{500} by adopting the Malmquist bias uncorrected L-M relation derived from the $M_{500} - Y_X$ relation with *self-similar slope* given in Eq. 3 of Arnaud et al. (2010). We find that for $\sim 96, 91\%$ of the clusters the difference is less than $5, 2\%$, respectively. The largest differences are found for low luminosity objects. In fact, if we consider clusters with $L_{500} \geq 10^{43}$ erg/s we find that for $\sim 99, 95\%$ of the clusters the difference is less than $5, 2\%$, respectively.

In order to explore the reliability of our assumption concerning the Malmquist bias correction of the L-M relation, we repeated our iterative procedure by using the *Malmquist bias corrected relation* of Pratt et al. (2009), finding essentially the same L_{500} (relative differences $\sim 1\%$). This is expected, because the steep drop of the typical cluster luminosity profile with radius makes L_{500} rather insensitive to the exact choice of R_{500} .

Using the two above-described methods we can therefore systematically compute L_{500} , the 0.1 – 2.4 keV energy band luminosities within R_{500} , for all the clusters (Table 3, L_500).

3.5. Total masses

Total masses M_{500} , estimated for the same cosmology adopted here, are directly available only for MACS_MJFV and MACS_BRIGHT clusters⁷. For almost all the clusters we therefore rely on luminosity as a mass proxy and estimate M_{500} (M_500 in Table 3) using Eq. 2. While our computation of L_{500} does not depend on the details of the adopted L-M relation (non-self-similarity of the underlying $M_{500} - Y_X$ relation and Malmquist bias correction), obviously the estimated M_{500} does. In particular, the M_{500} values provided by the MCXC rely on the assumption that on average the Malmquist bias for the samples used to construct the MCXC is the same as that of the REXCESS sample. Since the selection functions of the samples we use are complex (and indeed, in most cases are not known or available), our mass estimates must rely on this assumption. In addition, while our choice ensures maximal self-consistency in our modeling, other calibrations of the L-M relation could be adopted. Nevertheless, given our estimated L_{500} , the computation of total masses from a different L-M relation is straightforward.

From M_{500} we estimate the characteristic radii R_{500} (R_500 in Table 3) using:

$$M_{500} = (4\pi/3) \rho_c(z) 500 R_{500}^3, \quad (3)$$

where the critical density is $\rho_c(z) = 3H(z)^2/8\pi G$.

3.6. Notes

We gather together useful information concerning individual objects and add it to the MCXC as notes (NOTES in Table 3). In the input catalogues this information is usually provided as notes and comments and because it is different in type and size from catalogue to catalogue its homogenisation is not straightforward.

⁷ There are two exceptions (MACSJ0358.8-2955 and MACSJ2311.5+0338), but these clusters do not end up in the MCXC because they are also members of other catalogues.

In general, we choose not to include detailed and extended information and we therefore refer the reader to the cited papers for more information, e.g., the notes to Table 1 in Gioia & Luppino (1994) or in Table 2 of Romer et al. (2000a). In the following we describe the type of information we included in NOTES. For the meaning of abbreviations we refer the reader to the cited papers of each sub-catalogue.

For BCS, SGP, SHARC, NEP, MACS, CIZA, and EMSS no information is provided or is too detailed to be added in concisely. For NORAS we take information from column ID in Table 1 of Böhringer et al. (2000a) (information on source identification). For REFLEX, (Böhringer et al. 2004a), where the provided information is fairly detailed, we merge the following: (i) information in column Cm of Table 1 (information on source identification), (ii) the information concerning groupings as given in Table 10 with the simple note GR1, GR2, ..., GR10 if the cluster is listed in one of the 10 groupings listed in the table, (iii) multipeak information as given in Table 11 (columns Morphology and Orientation are merged, as e.g., two maxima/NE-SW), and (iv) information on whether the cluster is part of a line of sight structure as given in Table 12 (we simply add losStr if the cluster appears in the table). For 400SD clusters we take the information given in the column Notes in Table 4 of Burenin et al. (2007, information on alternative names is not used). For 160SD clusters we take the information given in the column Notes in Table 4 of Mullis et al. (2003, information on alternative names is not used).

3.7. Scale

In order to facilitate the conversion between angular and physical sizes (e.g., for R_{500}) we provide the angular scale factor SCALE in kpc/arcsec (see Table 3).

4. Duplicate clusters

The overlap between the survey areas of the input catalogues induces duplicate (and in some cases triplicate, quadruplicate, etc.) entries in the MCXC catalogue. In this Section we explain how these are identified and which entry is retained in the MCXC. In short, we search where a given cluster is a member of each input catalogue and, according to criteria based on the type of data and the size of the input catalogue, we retain only one entry in the MCXC. The full list of clusters without removal of multiple entries can be requested from the authors.

The most important criterion that we use to decide which duplicate cluster is preserved in the MCXC is the size of the input catalogue. In addition we give higher priority to catalogues that provide aperture luminosities because they ensure the most reliable and self-consistent computation of L_{500} . These two criteria allow us to rank the input catalogues from highest to lowest priority as in Table 1. Obviously, because of its size and the type of information it provides, NORAS/REFLEX is the catalogue with the highest priority. It is followed by other large and well-defined catalogues such as the 400SD, 160SD, BCS, etc. Hence, when a cluster is listed in more than one catalogue it is retained only as an entry in the input catalogue with higher priority. This catalogue ranking is not crucial for CIZA because the overlap of its survey area with other surveys is minimal.

Our procedure therefore reduces to the identification of multiple entries. This identification is based mainly on centroid coordinate differences, and to a lesser extent on redshift differences. Given the large number of entries, cluster identification is per-

formed in three steps in order to progressively reduce the number of candidate multiple entries.

1. In a first step if two clusters in different catalogues have centroid offsets of less than 1' and their relative redshift difference is less than 10 per cent they are identified as being the same cluster. Although this step removes a large number of duplicate entries, we compare their names and alternative names to make sure that we do not remove single entries. In the case of a doubtful association we do not remove any entry.
2. In a second step the resulting catalogue is inspected once more by carefully identifying clusters with centroid offsets of less than 5, 10, or even 20', and by varying the relative redshift difference. This time consuming procedure is needed because different source analysis techniques can yield rather different centroid positions, in particular for nearby clusters. Redshift differences can be very large and we use them only as indicators and not as stringent constraints. Each multiple entry candidate is checked, with names and alternative names used to facilitate the procedure. Again in this step we are rather conservative and do not remove any cluster if the identification is not certain.
3. In a third step the cleaned catalogue is inspected once more with large allowances for centroid offsets, and any overlaps are checked by visually inspecting RASS and PSPC maps. The associations inspected in this last step are either multiple systems or entries where very different redshifts are given for the same X-ray cluster.

In each of the three steps we make some exceptions to the general rules explained above. When the redshift difference is very large we keep the cluster with more recent or reliable redshift measurement. An extreme example is MCXC J1524.6+0957 (VMF98 170 or BVH2007 198), whose redshift is 0.07800 in SHARC and 0.5160 in 400SD. In this case, the average temperature of 5.1 keV measured by Vikhlinin et al. (2002) rules out the low redshift estimate. For double or multiple systems we retain measurements for each of the components instead of measurements of the whole system. This explains why, although it has the highest priority, the NORAS/REFLEX catalogue finally contains 10 clusters less than before our handling of duplicates. If possible, we compared our duplicates identifications with those in other work (e.g., Mullis et al. 2003) and find perfect agreement.

In order to retain useful information, when an entry with no available alternative name is kept in the MCXC catalogue while the one we discard provides it, we copy this information into the retained entry.

The MCXC provides information concerning multiple entries in the input catalogues through the label CAT_OV (see Table 3) which contains the name of the sub-catalogue from which the removed cluster entry is a member.

5. Discussion

5.1. Global catalogue characteristics

The final MCXC is constructed from the input catalogues discussed in Sect. 2 with information homogenised as explained in Sect. 3. Multiple entries in the resulting catalogue are handled as described in Sect. 4. This procedure yields the final MCXC catalogue, which comprises in total 1743 clusters (2397 initially, see Table 1) and contains virtually no multiple entries. In the

following we illustrate some basic properties of the MCXC. Notice that, because of the priorities we assign to the input catalogues, NORAS/REFLEX clusters constitute a large fraction of the MCXC (see Table 1).

The MCXC redshift histogram is illustrated in the bottom right hand panel of Fig. 1: 282, 77, and 18 clusters ($\sim 16, 4, 1$ per cent, respectively) have redshifts larger than 0.3, 0.5 and 0.7. In Fig 3 we show the number of clusters as a function of luminosity: 846, 64 ($\sim 49, 4$ per cent, respectively) of the clusters have 0.1–2.4 keV band luminosities L_{500} larger than 1, 10×10^{44} erg/s. In Fig. 4 we show the 0.1 – 2.4 keV band luminosities L_{500} of

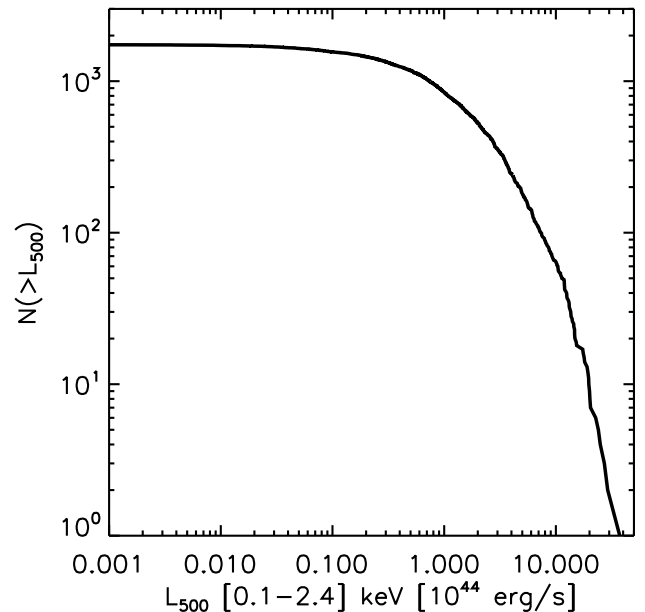


Fig. 3. Luminosity distribution of MCXC clusters.

the 1743 MCXC clusters as a function of redshift in log-log (top panel) and the more conventional lin-log scale (bottom panel). These figures highlight both the different nature of RASS-based and serendipitous surveys and their complementarity. For a given redshift, serendipitously discovered clusters are less luminous than those from RASS-based catalogues because the deeper exposures allow lower flux limits to be adopted. This implies that the fraction of high redshift clusters in serendipitous surveys is much higher than that of RASS-based surveys.

In addition to redshift and luminosity (and total mass), a fundamental quantity provided by the MCXC is the cluster position in the sky, both in equatorial and galactic coordinates. In Fig. 5 we show the distribution on the sky of the 1743 MCXC clusters in galactic coordinates. Some distinctive features are: NORAS/REFLEX, BCS and MACS clusters are fairly homogeneously distributed; the only clusters at low galactic latitude are from the CIZA survey; the RASS-based clusters of SGP and NEP are localised in narrow regions; serendipitous clusters are sparsely distributed across the sky.

5.2. Robustness of luminosity measurements

As the luminosity L_{500} the most relevant physical quantity provided by the MCXC, we focus on its discussion in the remainder of this Section.

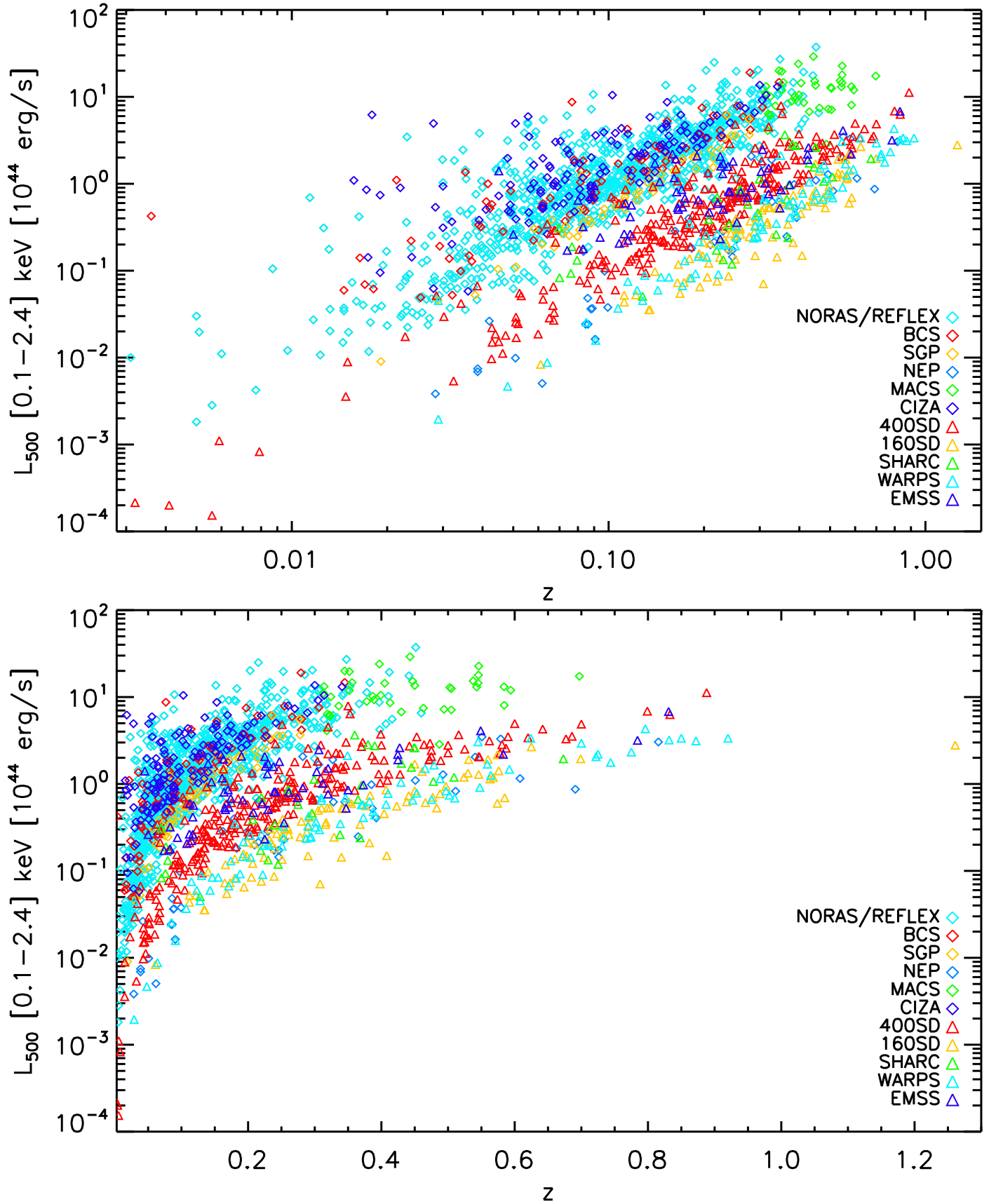


Fig. 4. *Top:* The 0.1 – 2.4 keV band luminosities L_{500} of the 1743 MCXC clusters as a function of redshift. Diamonds and triangles indicate clusters from RASS-based and serendipitous catalogues, respectively. *Bottom:* Same, but in lin-log scale.

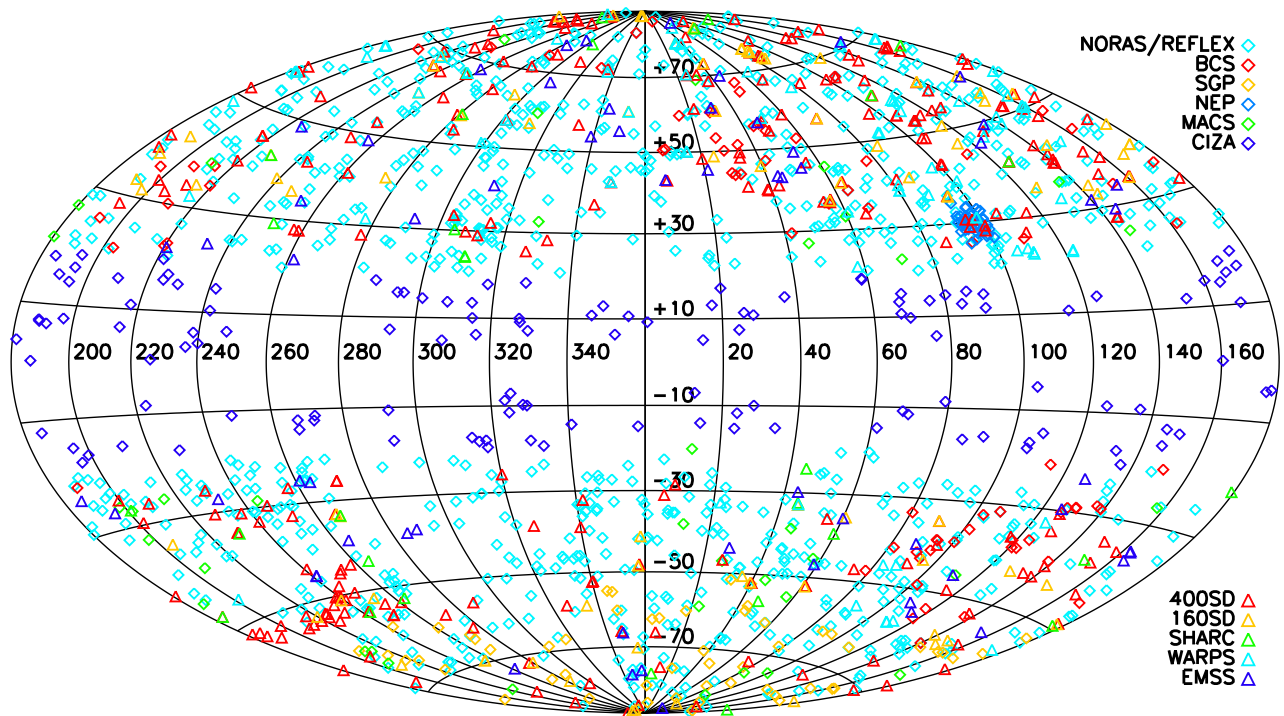


Fig. 5. Sky map of the 1743 MCXC clusters in galactic coordinates. Symbols and colors are the same as in Fig. 4.

Since the modeling adopted in Sect. 3 is based on results from the REXCESS sample, and that the latter is a subsample of REFLEX, the comparison of the L_{500} values derived in this work and those given in Pratt et al. (2009) for the 31 REXCESS clusters provides a useful test for our procedure. We remind the reader that for all the REFLEX clusters we computed the luminosities L_{500} from aperture luminosities by means of the iterative procedure explained in Sect. 3. We find that our derived R_{500} is larger than R_{ap} for only seven REXCESS clusters, and at most only by ~ 20 per cent. In Fig. 6 we show the ratio between our estimate of L_{500} and the *XMM-Newton* measurements given in Pratt et al. (2009), $L_{500,\text{REXCESS}}$. Uncertainties on the luminosity ratios are computed from quadratic sum of the errors given in Pratt et al. (2009) and propagation of the aperture luminosity errors provided in Böhringer et al. (2004a). Notice that for one cluster the redshift adopted in our work differs from the one used in $L_{500,\text{REXCESS}}$. Although we correct for this difference, this has no impact on our results. Symbols in Fig. 6 are as in Pratt et al. (2009), i.e. blue stars for cool core clusters and red squares for morphologically disturbed clusters. We compute error weighted means and standard deviations of the luminosity ratio and find: 0.965 ± 0.141 for all 31 clusters, 0.932 ± 0.078 for the cool core clusters, and 0.951 ± 0.193 for the disturbed clusters. Our comparison indicates a good agreement between the two measurements. Notice the fairly large scatter at low luminosity, the large scatter for disturbed clusters with respect to cool core clusters, and that there is an indication that our luminosity estimates are on average biased low in cool core systems (a 1σ effect). The lower luminosity ratio for cool core clusters is expected because they are modeled using the AB-model derived from the mean of

the REXCESS sample (Eq. 1), although their emission is more centrally peaked. We find no trend of luminosity ratio with the ratio R_{ap}/R_{500} and no redshift dependence as the REXCESS sample redshift leverage is too small.

5.3. Intercomparison of original luminosity measurements

The procedure adopted to handle multiple entries (detailed in Sect. 4) allows us to compare L_{500} estimates derived from different input luminosity measurements. A total of 558 MCXC entries list the properties of a cluster that is a member of more than one input catalogue, and for which only the information from only one input catalogue has been retained. For these entries there are therefore N luminosity measurements (one provided by the MCXC and $N-1$ unused overlaps) of the 0.1 – 2.4 keV band luminosity L_{500} . There are 5 clusters with $N = 5$, 8 with $N = 4$, 59 with $N = 3$, and 486 with $N = 2$.

The luminosities L_{500} are compared as follows. For each of the 558 entries we compute the ratio $L_{500}/L_{500,\text{MCXC}}$ where $L_{500,\text{MCXC}}$ is the luminosity given in the MCXC and L_{500} is the luminosity of the same cluster, but derived from a different input catalogue (i.e., the overlap luminosity). As explained in Sect. 4, in some cases the redshifts provided by the input catalogues can be fairly different. We therefore correct the luminosities of the overlaps by multiplying them with the squared ratio of the luminosity distances at the two different redshifts. This is equivalent to comparing the 0.1 – 2.4 keV band fluxes within R_{500} . The MCXC provides these luminosity ratios through the quantity L_{500_RAT} (see Table 3) where they are ordered in the same way as the sub-catalogue names in `CAT_OV`.

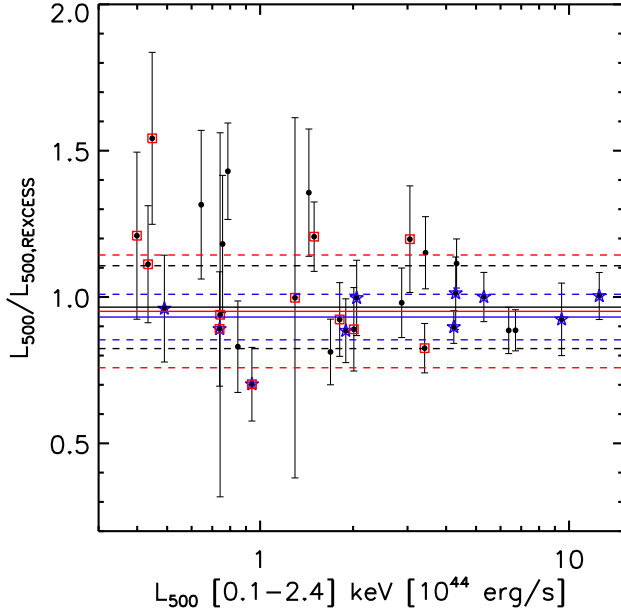


Fig. 6. Ratio $L_{500}/L_{500,REXCESS}$ between our estimate of the 0.1–2.4 keV band luminosities L_{500} and the *XMM-Newton* measurements of Pratt et al. (2009) as a function of L_{500} . Blue stars indicate cool core clusters while red squares morphologically disturbed clusters. Solid lines indicate error weighted means and dashed lines represent the error weighted means \pm error weighted standard deviations (black for all clusters, blue for cool core clusters, and red for morphologically disturbed clusters as defined in Pratt et al. (2009)).

In Fig. 7 we show the luminosity L_{500} of the overlaps (top panel) and the ratio $L_{500}/L_{500,MCXC}$ (bottom panel, in dex units) as a function of $L_{500,MCXC}$. Both a direct fit to the data (which is shown in the top panel of the figure and basically indistinguishable from equality) and the mean value of the luminosity ratios indicate that the different luminosity determinations are in excellent agreement. In particular, in order to avoid any bias introduced by the wide range of luminosity values, we compute the ratios of the log values of the luminosities. The error weighted mean and standard deviation of these ratios are adopted to quantify the agreement between the different luminosity estimates. Errors are computed from the uncertainties quoted in the input catalogues, assuming that the relative error on the luminosities L_{500} is the same as the one on the input luminosities. We find 0.999 and 0.003 for the error weighted mean and standard deviation, respectively. We performed the same analysis by taking into account whether the compared luminosities are derived from RASS or pointed observations and whether they are computed iteratively or just by adopting a constant conversion factor (see Sect. 3) and find no significant trend. The luminosity comparison therefore shows that on average the agreement between different L_{500} measurements is excellent. However, the clear outliers in Fig. 7 indicate that for some clusters there are large discrepancies.

Although a discussion on individual objects, and thus on the difference between specific survey measurements, is beyond the scope of our work, we briefly discuss very discrepant luminosity estimates by focussing on strong outliers with luminosity ratios larger than 2 or smaller 0.5 in Fig. 7 (i.e., differences larger than

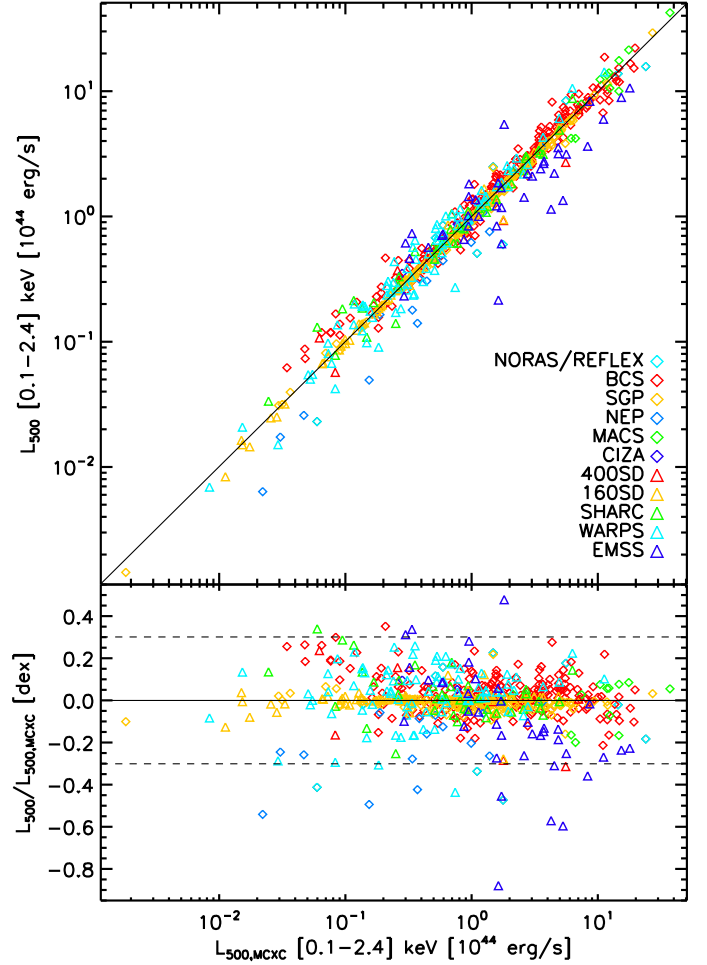


Fig. 7. Luminosity L_{500} of the overlaps (top panel) and the ratio $L_{500}/L_{500,MCXC}$ in dex (bottom panel) as a function of $L_{500,MCXC}$, the luminosity measurements retained in the MCXC. Symbols and colors are the same as in Fig. 4, but refer to the overlaps only. The solid line in the top panel indicates the best fit to the data. The solid line in the bottom panel indicates the error weighted mean of the luminosity ratio, while the dashed horizontal lines indicates the luminosity ratios equal to 2 and 0.5.

a factor of 2). There is a total of twenty objects (~ 4 per cent of those with more than one luminosity measurement) of such discrepant estimates. For six of these clusters, three luminosity estimates are available. Interestingly, of these, we always find that only one of the three is very different from the others, and that the two remaining estimates agree within a few percent. For the other fourteen clusters only two estimates of L_{500} are available. Of these, five involve measurements from the EMSS and seven are faint objects at low redshift, where extrapolation might strongly affect the luminosity estimates. For the remaining two clusters (A2507 and RXC J1003.0+3254) we find no obvious explanation.

6. Summary and conclusions

Motivated by the strong need for a large, homogeneous compilation in the framework of X-ray, SZ and other multi-wavelength studies, we have presented the construction and properties of the MCXC, a Meta-Catalogue of X-ray detected Clusters of

galaxies. The MCXC is constructed from publicly-available RASS-based (NORAS, REFLEX, BCS, SGP, NEP, MACS, and CIZA) and serendipitous (160SD, 400SD, SHARC, WARPS, and EMSS) cluster catalogues (see Sect. 2). The information from these input catalogues is systematically homogenised using the most up to date knowledge of the structural properties and scaling relations of X-ray clusters, and is undertaken in a self-consistent way (see Sect. 3). More specifically, in addition to the fairly straightforward standardisation of quantities such as coordinates and redshifts (RAJ2000, DEJ2000, etc., and Z in Tables 2 and 3), we converted the available luminosities to 0.1 – 2.4 keV band luminosities L_{500} (L_{500} in Table 3) by adopting the average gas density profile (Croston et al. 2008) and L-M relation (Pratt et al. 2009) derived from the representative X-ray cluster sample REXCESS. The computation is performed directly from aperture luminosities when available (~ 76 per cent of the MCXC clusters) and we verify that the derived luminosities do not depend on the details of the adopted L-M relation.

Total masses M_{500} and radii R_{500} can be computed from the luminosities L_{500} by adopting an L-M relation. The MCXC provides these quantities computed self-consistently using the L-M relation adopted in this work (M_{500} and R_{500} in Table 3). The MCXC further provides three cluster identifiers: the MCXC name, the original name as given in the input catalogues, and an alternative name ($NAME_MCXC$, $NAME$, and $NAME_ALT$ in Table 2, respectively). The latter has been homogenised to match both SIMBAD and NED standards. In addition, we collated important information usually provided as notes and comments in the input catalogues ($NOTES$ in Table 3).

Multiple entries originating from overlaps between the survey areas of the input catalogues are very carefully handled (see Sect. 4). The result of this procedure is provided by the MCXC (CAT_OV in Table 3). We compare luminosity measurements from different catalogues, finding that on average the agreement is excellent, and discuss the most discrepant measurements (see Sect. 5). We find good agreement with the precisely measured REXCESS luminosities given in Pratt et al. (2009). These comparisons strongly support the validity of our approach. The MCXC provides the luminosity ratios for clusters that appear in multiple input catalogues (see L_{500_RAT} in Table 3).

The MCXC comprises 1743 clusters ordered by right ascension, and contains virtually no multiple entries. The full MCXC is available at CDS⁸ and contains the information given in Columns (1)-(19) in Tables 2 and 3, where the first 40 entries are given as an example.

We envisage that the catalogue will be useful for the construction of representative samples for work on structural properties and samples for cosmological investigations; examination of SZ-X-ray scaling relations; checking of SZ candidates; selection function studies; definition of samples for lensing and optical/IR follow-up. The work by Melin et al. (2010) is an example of how the information provided by the MCXC can be used for SZ studies. In particular, their work illustrates that given the MCXC luminosities, the universal pressure profile and the associated SZ scaling relations provided by Arnaud et al. (2010) yield the X-ray predicted SZ signal from individual objects, which can be then compared to those observed with WMAP. This approach will be extremely useful for studies based on SZ surveys such as Planck, SPT, and ACT.

The MCXC is an ongoing project and will be extended to include available data for individual clusters at high redshift (the most relevant for cosmological studies) and cluster catalogues

derived from ongoing X-ray surveys when they are publicly available.

Acknowledgements. We thank Isabella Gioia, Patrick Henry, and Donald Horner for helpful discussions and Nabila Aghanim for strongly supporting the project. This research has made use of the VizieR database, operated at CDS, Strasbourg. EP acknowledges the support of grant ANR-06-JCJC-0141.

References

- Andersson, K., Benson, B. A., Ade, P. A. R., et al. 2010, *ApJ*, submitted (arXiv:1006.3068)
- Arnaud, M., Pointecouteau, E., & Pratt, G. W. 2007, *A&A*, 474, L37
- Arnaud, M., Pratt, G. W., Piffaretti, R., et al. 2009, *A&A*, in press (arXiv:0910.1234)
- Barkhouse, W. A., Green, P. J., Vikhlinin, A., et al. 2006, *ApJ*, 645, 955
- Böhringer, H., Briel, U. G., Schwarz, R. A., et al. 1994, *Nature*, 368, 828
- Böhringer, H., Voges, W., Huchra, J. P., et al. 2000, *ApJS*, 129, 435
- Böhringer, H., Voges, W., Huchra, J. P., et al. 2000, *VizieR Online Data Catalog*, 212, 90435
- Böhringer, H., Schuecker, P., Guzzo, L., et al. 2004, *A&A*, 425, 367
- Böhringer, H., Schuecker, P., Guzzo, L., et al. 2004, *VizieR Online Data Catalog*, 342, 50367
- Böhringer, H., Schuecker, P., Pratt, G. W., et al. 2007, *A&A*, 469, 363
- Burenin, R. A., Vikhlinin, A., Hornstrup, A., et al. 2007, *ApJS*, 172, 561
- Burenin, R. A., Vikhlinin, A., Hornstrup, A., et al. 2009, *VizieR Online Data Catalog*, 217, 20561
- Burke, D. J., Collins, C. A., Sharples, R. M., Romer, A. K., & Nichol, R. C. 2003, *MNRAS*, 341, 1093
- Burke, D. J., Collins, C. A., Sharples, R. M., Romer, A. K., & Nichol, R. C. 2003, *VizieR Online Data Catalog*, 734, 11093
- Carlstrom, J. E., Ade, P. A. R., Aird, K. A., et al. 2009, *PASP*, submitted (arXiv:0907.4445)
- Croston, J. H., Pratt, G. W., Böhringer, H., et al. 2008, *A&A*, 487, 431
- Craddace, R., Voges, W., Böhringer, H., et al. 2002, *ApJS*, 140, 239
- Craddace, R., Voges, W., Böhringer, H., et al. 2002, *VizieR Online Data Catalog*, 214, 239
- Craddace, R., Voges, W., Böhringer, H., et al. 2003, *ApJS*, 144, 299
- Ebeling, H., Edge, A. C., Böhringer, H., et al. 1998, *MNRAS*, 301, 881
- Ebeling, H., Edge, A. C., Allen, S. W., et al. 2000, *MNRAS*, 318, 333
- Ebeling, H., Edge, A. C., Böhringer, H., et al. 2000, *VizieR Online Data Catalog*, 730, 10881
- Ebeling, H., Edge, A. C., Allen, S. W., et al. 2000, *VizieR Online Data Catalog*, 731, 80333
- Ebeling, H., Edge, A. C., & Henry, J. P. 2001, *ApJ*, 553, 668
- Ebeling, H., Mullis, C. R., & Tully, R. B. 2002, *ApJ*, 580, 774
- Ebeling, H., Barrett, E., Donovan, D., et al. 2007, *ApJ*, 661, L33
- Ebeling, H., Edge, A. C., Mantz, A., et al. 2010, *MNRAS*, in press (arXiv:1004.4683)
- Evrard, A. E., Metzler, C. A., & Navarro, J. F. 1996, *ApJ*, 469, 494
- Fassbender, R., 2008, PhD thesis (astro-ph/0806.0861v1)
- Fowler, J. W., Niemack, M. D., Dicker, S. R., et al. 2007, *Appl. Opt.*, 46, 3444
- Gioia, I. M., Maccacaro, T., Schild, R. E., et al. 1990, *ApJS*, 72, 567
- Gioia, I. M., & Luppino, G. A. 1994, *ApJS*, 94, 583
- Henry, J. P. 2000, *ApJ*, 534, 565
- Henry, J. P. 2004, *ApJ*, 609, 603
- Henry, J. P., Mullis, C. R., Voges, W., et al. 2006, *ApJS*, 162, 304
- Horner, D. J., Perlman, E. S., Ebeling, H., et al. 2008, *ApJS*, 176, 374
- Horner, D. J., Perlman, E. S., Ebeling, H., et al. 2009, *VizieR Online Data Catalog*, 217, 60374
- Kocevski, D. D., Ebeling, H., Mullis, C. R., & Tully, R. B. 2007, *ApJ*, 662, 224
- Komatsu, E., Smith, K. M., Dunkley, J., et al. 2010, *ApJSS*, submitted (arXiv:1001.4538)
- Kravtsov, A. V., Vikhlinin, A., & Nagai, D. 2006, *ApJ*, 650, 128
- Liedahl, D. A., Osterheld, A. L., & Goldstein, W. H. 1995, *ApJ*, 438, L115
- Mahdavi, A., Hoekstra, H., Babul, A., & Henry, J. P. 2008, *MNRAS*, 384, 1567
- Majumdar, S., & Mohr, J. J. 2003, *ApJ*, 585, 603
- Mantz, A., Allen, S. W., Rapetti, D., & Ebeling, H. 2009, *MNRAS*, submitted (arXiv:0909.3098)
- Mantz, A., Allen, S. W., Ebeling, H., Rapetti, D., & Drlica-Wagner, A. 2009, *MNRAS*, submitted (arXiv:0909.3099)
- Markevitch, M., & Vikhlinin, A. 2007, *Phys. Rep.*, 443, 1
- Maughan, B. J. 2007, *ApJ*, 668, 772
- Maughan, B. J., Jones, C., Forman, W., & Van Speybroeck, L. 2008, *ApJS*, 174, 117
- McNamara, B. R., & Nulsen, P. E. J. 2007, *ARA&A*, 45, 117
- Melin, J.-B., Bartlett, J. G., & Delabrouille, J. 2006, *A&A*, 459, 341

⁸ <http://cds.u-strasbg.fr/>

- Melin, J.-B., Bartlett, J. G., Delabrouille, J., et al. 2010, A&A, submitted (arXiv: 1001.0871)
- Menanteau, F., Gonzalez, J., Juin, J.-B., et al. 2010, ApJ, submitted (arXiv: 1006.5126)
- Meneghetti, M., Rasia, E., Merten, J., et al. 2010, A&A, 514, A93
- Mewe, R., Gronenschild, E. H. B. M., & van den Oord, G. H. J. 1985, A&AS, 62, 197
- Mullis, C. R., McNamara, B. R., Quintana, H., et al. 2003, ApJ, 594, 154
- Nagai, D., Vikhlinin, A., & Kravtsov, A. V. 2007, ApJ, 655, 98
- Pacaud, F., Pierre, M., Refregier, A., et al. 2007, MNRAS, 382, 1289
- Perlman, E. S., Horner, D. J., Jones, L. R., et al. 2002, ApJS, 140, 265
- Perlman, E. S., Horner, D. J., Jones, L. R., et al. 2002, VizieR Online Data Catalog, 214, 265
- Piffaretti, R., & Valdarnini, R. 2008, A&A, 491, 71
- Popesso, P., Böhringer, H., Brinkmann, J., Voges, W., & York, D. G. 2004, A&A, 423, 449
- Pratt, G. W., & Arnaud, M. 2002, A&A, 394, 375
- Pratt, G. W., Croston, J. H., Arnaud, M., Böhringer, H. 2009, A&A, 498, 361
- Pratt, G. W., Arnaud, M., Piffaretti, R., et al. 2010, A&A, 511, A85
- Rasia, E., Ettori, S., Moscardini, L., et al. 2006, MNRAS, 369, 2013
- Romer, A. K., Nichol, R. C., Holden, B. P., et al. 2000, ApJS, 126, 209
- Romer, A. K., Nichol, R. C., Holden, B. P., et al. 2000, VizieR Online Data Catalog, 212, 60209
- Romer, A. K., Viana, P. T. P., Liddle, A. R., & Mann, R. G. 2001, ApJ, 547, 594
- Rosati, P., della Ceca, R., Norman, C., & Giacconi, R. 1998, ApJ, 492, L21
- Rosati, P., Borgani, S., & Norman, C. 2002, ARA&A, 40, 539
- Šuhada, R., Song, J., Böhringer, H., et al. 2010, A&A, 514, L3
- Sunyaev, R. A., & Zel'dovich, Y. B. 1972, Comments on Astrophysics and Space Physics, 4, 173
- Tauber, J. A., Mandolesi, N., Puget, J.-L., et al. 2010, A&A, in press
- Vanderlinde, K., Crawford, T. M., de Haan, T., et al. 2010, ApJ, submitted (arXiv: 1003.0003)
- Vikhlinin, A., van Speybroeck, L., Markevitch, M., Forman, W. R., & Grego, L. 2002, ApJ, 578, L107
- Vikhlinin, A., Kravtsov, A., Forman, W. R. 2006, ApJ, 640, 691
- Vikhlinin, A., Burenin, R. A., Ebeling, H., et al. 2009, ApJ, 692, 1033
- Voges, W., Aschenbach, B., Böller, T., et al. 1999, A&A, 349, 389
- Voit, G. M. 2005, Reviews of Modern Physics, 77, 207
- Zhang, Y.-Y., Okabe, N., Finoguenov, A., et al. 2010, ApJ, 711, 1033

Table 2. The first 40 entries of the MCXC catalogue. The full MCXC is available at CDS.

NAME_MCXC	NAME	NAME_ALT	RAJ2000	DEJ2000	_RAJ2000	_DEJ2000	GLON	GLAT	Z	CATALOGUE	SUB_CATALOGUE
MCXC name	Name	Alternative name	Right ascension (J2000)	Declination (J2000)	Right ascension (deg)	Declination (deg)	Galactic longitude (deg)	Galactic latitude (deg)	Redshift	Catalogue name	Sub-catalogue name
(1)	(2)	(3)	(4)	(5)	(6)	(7)	(8)	(9)	(10)	(11)	(12)
MCXC J0000.1+0816	RXC J0000.1+0816	UGC 12890	00 00 07.1	08 16 27.8	0.030	8.274	101.783	-52.477	0.0396	NORAS/REFLEX	NORAS
MCXC J0000.4-0237	RXC J0000.4-0237		00 00 24.7	-02 37 30.0	0.103	-2.625	94.268	-62.622	0.0379	SGP	SGP
MCXC J0001.6-1540	RXC J0001.6-1540		00 01 39.0	-15 40 52.0	0.413	-15.681	75.129	-73.733	0.1246	SGP	SGP
MCXC J0001.9+1204	RXC J0001.9+1204	A2692	00 01 57.0	12 04 22.8	0.488	12.073	104.308	-49.001	0.2033	NORAS/REFLEX	NORAS
MCXC J0003.1-0605	J0003.1-0605	A2697	00 03 11.8	-06 05 09.6	0.799	-6.086	92.169	-66.033	0.2320	NORAS/REFLEX	REFLEX
MCXC J0003.2-3555	J0003.2-3555	A2717	00 03 12.1	-35 55 37.6	0.801	-35.927	349.330	-76.490	0.0490	NORAS/REFLEX	REFLEX
MCXC J0003.8+0203	J0003.8+0203	A2700	00 03 50.6	02 03 48.2	0.961	2.063	99.610	-58.637	0.0924	NORAS/REFLEX	REFLEX
MCXC J0004.9+1142	RXC J0004.9+1142	UGC 00032	00 04 59.4	11 42 02.2	1.247	11.701	105.239	-49.569	0.0761	NORAS/REFLEX	NORAS
MCXC J0005.3+1612	RXC J0005.3+1612	A2703	00 05 22.6	16 12 37.8	1.344	16.211	107.133	-45.244	0.1164	NORAS/REFLEX	NORAS
MCXC J0006.0-3443	J0006.0-3443	A2721	00 06 03.0	-34 43 26.8	1.513	-34.724	352.147	-77.668	0.1147	NORAS/REFLEX	REFLEX
MCXC J0006.3+1052	RXC J0006.3+1052	ZwCl15	00 06 21.7	10 52 03.7	1.591	10.868	105.386	-50.462	0.1698	NORAS/REFLEX	NORAS
MCXC J0008.9+4110	ZwCl28	ZwCl28	00 08 56.9	41 10 37.2	2.237	41.177	114.386	-20.989	0.1537	BCS	eBCS
MCXC J0009.7-3516	MS0007.2-3532		00 09 46.5	-35 16 30.0	2.444	-35.275	347.884	-77.942	0.0500	EMSS	EMSS_1994
MCXC J0011.3-2851	J0011.3-2851	A2734	00 11 20.7	-28 51 18.4	2.836	-28.855	19.562	-80.986	0.0620	NORAS/REFLEX	REFLEX
MCXC J0011.7-1523	MACSJ0011.7-1523		00 11 42.8	-15 23 22.0	2.928	-15.389	82.746	-75.067	0.3780	MACS	MACS_BRIGHT
MCXC J0011.7+3225	RXC J0011.7+3225	A0007	00 11 44.4	32 25 01.2	2.935	32.417	113.289	-29.710	0.1073	NORAS/REFLEX	NORAS
MCXC J0013.6-1930	J0013.6-1930	A0013	00 13 38.3	-19 30 07.6	3.409	-19.502	72.276	-78.456	0.0940	NORAS/REFLEX	REFLEX
MCXC J0014.3-6604	J0014.3-6604	A2746	00 14 18.4	-66 04 39.0	3.577	-66.078	308.850	-50.622	0.1599	NORAS/REFLEX	REFLEX
MCXC J0014.3-3023	J0014.3-3023	A2744	00 14 18.8	-30 23 00.2	3.578	-30.383	8.936	-81.240	0.3066	NORAS/REFLEX	REFLEX
MCXC J0014.3+0854	MS0011.7+0837		00 14 19.8	08 54 00.0	3.583	8.900	107.635	-52.866	0.1630	EMSS	EMSS_1994
MCXC J0015.4-2350	J0015.4-2350	A14	00 15 24.0	-23 50 42.0	3.850	-23.845	52.930	-81.233	0.0645	NORAS/REFLEX	REFLEX
MCXC J0015.9+1614	MS0013.4+1558		00 15 55.9	16 14 57.5	3.983	16.249	110.669	-45.775	0.0830	EMSS	EMSS_1994
MCXC J0016.3-3121	RXC J0016.3-3121	A2751	00 16 19.8	-31 21 55.1	4.083	-31.365	1.882	-81.252	0.0805	SGP	SGP
MCXC J0016.7+0646	RXC J0016.7+0646	A0016	00 16 45.5	06 46 25.0	4.190	6.774	107.775	-55.074	0.0833	NORAS/REFLEX	NORAS
MCXC J0017.5-3509	J0017.5-3509	A2755	00 17 33.7	-35 09 54.0	4.390	-35.165	342.856	-79.187	0.0968	NORAS/REFLEX	REFLEX
MCXC J0018.5+1626	MACSJ0018.5+1626	CL 0016+1609	00 18 33.8	16 26 16.6	4.641	16.438	111.609	-45.710	0.5456	MACS	MACS_DIST
MCXC J0019.0-2026	RXC J0019.0-2026	S26	00 19 03.9	-20 26 17.2	4.766	-20.438	73.324	-80.025	0.2773	SGP	SGP
MCXC J0019.6+2517	RXC J0019.6+2517		00 19 39.1	25 17 26.9	4.913	25.291	113.924	-37.024	0.1353	NORAS/REFLEX	NORAS
MCXC J0020.1+0005	RXC J0020.1+0005		00 20 10.7	00 05 30.1	5.044	0.092	106.230	-61.762	0.2124	NORAS/REFLEX	NORAS
MCXC J0020.5-4913	RXC J0020.5-4913	A2764	00 20 34.1	-49 13 40.1	5.142	-49.228	315.963	-67.112	0.0711	SGP	SGP
MCXC J0020.6+2840	RXC J0020.6+2840	A0021	00 20 40.9	28 40 30.4	5.171	28.675	114.819	-33.712	0.0940	NORAS/REFLEX	NORAS
MCXC J0020.7-2542	J0020.7-2542	A0022	00 20 42.8	-25 42 37.1	5.179	-25.710	42.851	-82.978	0.1410	NORAS/REFLEX	REFLEX
MCXC J0021.5+2803	RXC J0021.5+2803	IV Zw 015	00 21 35.9	28 03 04.7	5.400	28.051	114.954	-34.358	0.0948	NORAS/REFLEX	NORAS
MCXC J0022.0+0422	J0022.0+0422	GHO 00190.5+0405	00 22 03.4	04 22 37.9	5.514	4.377	109.128	-57.705	0.4070	WARPS	WARPS
MCXC J0023.1+0421	J0023.1+0421		00 23 06.0	04 21 13.0	5.775	4.354	109.596	-57.783	0.4530	WARPS	WARPS
MCXC J0024.0-1704	RXC J0024.0-1704	A2768	00 24 03.6	-17 04 32.2	6.015	-17.076	89.329	-78.121	0.1890	SGP	SGP
MCXC J0024.5+3312	RXC J0024.5+3312		00 24 31.8	33 12 31.3	6.133	33.209	116.478	-29.326	0.2260	NORAS/REFLEX	NORAS
MCXC J0025.4-1222	MACSJ0025.4-1222		00 25 29.4	-12 22 37.1	6.372	-12.377	99.264	-74.044	0.5843	MACS	MACS_DIST
MCXC J0025.5-3302	J0025.5-3302	S0041	00 25 32.4	-33 02 49.9	6.385	-33.047	344.774	-81.854	0.0491	NORAS/REFLEX	REFLEX
MCXC J0026.7+0501	J0026.7+0501	GHO 0024+0444	00 26 47.8	05 01 25.7	6.699	5.024	111.519	-57.301	0.2529	WARPS	WARPSII

Table 3. The first 40 entries of the MCXC catalogue, continued.

NAME_MCXC	Z	SCALE	L_500	M_500	R_500	NOTES	CAT_OV	L_500_rat
MCXC name	Redshift	Scale	L_{500}	M_{500}	R_{500}	Notes	Catalogues overlap	$L_{500}/L_{500,MCXC}$
		(kpc/'')	(10^{44} erg/s)	($10^{14} M_{\odot}$)	(Mpc)			
		(13)	(14)	(15)	(16)	(17)	(18)	(19)
MCXC J0000.1+0816	0.0396	0.784	0.196	0.737	0.630		BCS	1.084
MCXC J0000.4-0237	0.0379	0.752	0.052	0.330	0.482			
MCXC J0001.6-1540	0.1246	2.234	0.815	1.656	0.802			
MCXC J0001.9+1204	0.2033	3.342	1.990	2.693	0.918			
MCXC J0003.1-0605	0.2320	3.698	6.107	5.219	1.133			
MCXC J0003.2-3555	0.0490	0.959	0.442	1.202	0.739	losStr	SGP	0.952
MCXC J0003.8+0203	0.0924	1.719	0.847	1.734	0.823		SGP	0.886
MCXC J0004.9+1142	0.0761	1.443	0.519	1.301	0.752		eBCS SGP	0.920 0.922
MCXC J0005.3+1612	0.1164	2.107	1.579	2.493	0.922	B	eBCS	0.967
MCXC J0006.0-3443	0.1147	2.080	1.809	2.712	0.949		EMSS_1994	0.533
MCXC J0006.3+1052	0.1698	2.895	2.273	2.994	0.962		SGP	0.949
MCXC J0008.9+4110	0.1537	2.668	2.111	2.896	0.957		eBCS	0.933
MCXC J0009.7-3516	0.0500	0.977	0.262	0.873	0.664			
MCXC J0011.3-2851	0.0620	1.195	1.086	2.061	0.881	losStr	SGP	0.914
MCXC J0011.7-1523	0.3780	5.188	8.900	7.200	1.190			
MCXC J0011.7+3225	0.1073	1.962	2.572	3.378	1.023		BCS	1.042
MCXC J0013.6-1930	0.0940	1.746	1.236	2.182	0.888	losStr	SGP	0.955
MCXC J0014.3-6604	0.1599	2.756	2.827	3.446	1.012	X		
MCXC J0014.3-3023	0.3066	4.522	11.818	7.361	1.236		SGP MACS_BRIGHT	0.985 1.139
MCXC J0014.3+0854	0.1630	2.800	1.928	2.722	0.934			
MCXC J0015.4-2350	0.0645	1.240	0.326	0.988	0.689	X	SGP	0.956
MCXC J0015.9+1614	0.0830	1.561	0.320	0.964	0.679			
MCXC J0016.3-3121	0.0805	1.518	0.495	1.261	0.743			
MCXC J0016.7+0646	0.0833	1.566	0.319	0.963	0.679		eBCS	1.385
MCXC J0017.5-3509	0.0968	1.792	0.692	1.529	0.788	losStr	SGP	0.964
MCXC J0018.5+1626	0.5456	6.386	17.911	7.785	1.148		EMSS_2004	0.593
MCXC J0019.0-2026	0.2773	4.215	5.571	4.763	1.081			
MCXC J0019.6+2517	0.1353	2.397	1.442	2.327	0.895			
MCXC J0020.1+0005	0.2124	3.458	0.687	1.398	0.735			
MCXC J0020.5-4913	0.0711	1.356	0.268	0.873	0.659			
MCXC J0020.6+2840	0.0940	1.746	1.435	2.389	0.916		BCS	1.201
MCXC J0020.7-2542	0.1410	2.482	2.872	3.527	1.026		SGP	0.912
MCXC J0021.5+2803	0.0948	1.759	0.968	1.878	0.845		BCS	0.956
MCXC J0022.0+0422	0.4070	5.430	0.582	1.082	0.628			
MCXC J0023.1+0421	0.4530	5.781	0.785	1.250	0.647			
MCXC J0024.0-1704	0.1890	3.156	1.484	2.276	0.872			
MCXC J0024.5+3312	0.2260	3.626	2.993	3.394	0.983			
MCXC J0025.4-1222	0.5843	6.603	8.042	4.623	0.950			
MCXC J0025.5-3302	0.0491	0.961	0.495	1.287	0.756		SGP	0.929
MCXC J0026.7+0501	0.2529	3.943	0.326	0.860	0.616			

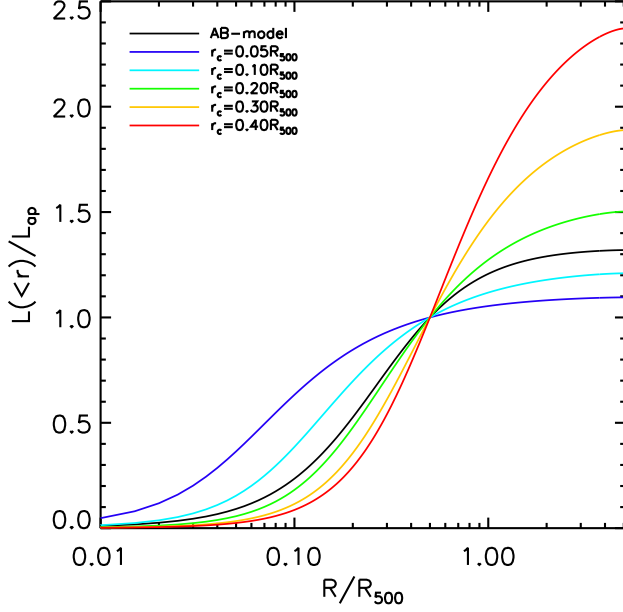


Fig. A.1. Luminosity radial profile normalised at $R_{\text{ap}} = 0.5 \times R_{500}$ for the AB-model (black line) and β -models with different core radii (color lines).

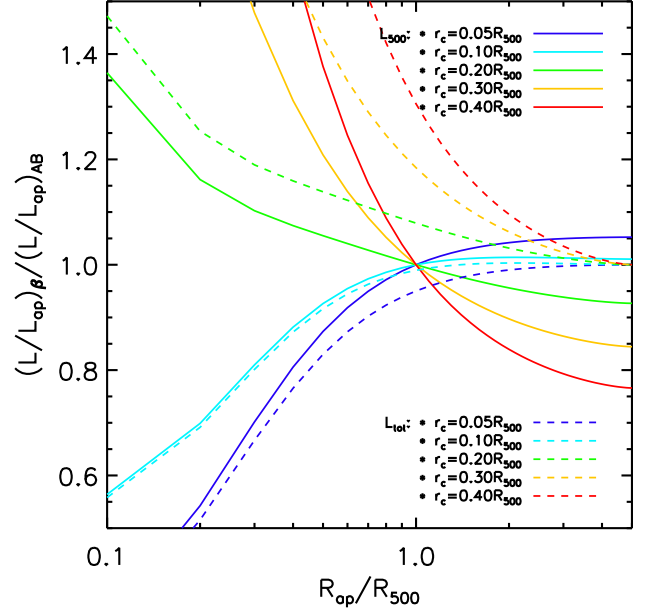


Fig. A.2. The β -model to AB-model ratio of the normalised luminosity profile L/L_{ap} evaluated at R_{500} (solid lines) and $5 \times R_{500}$ (dashed lines) as a function of R_{ap} .

Appendix A: AB-model versus β -model luminosity profiles

In the following we illustrate the difference between predictions based on the AB-model and a 'typical' β -model. In particular we focus on L_{500} and total luminosities L_{tot} estimated from a given aperture luminosity.

The AB-model adopted in this work is given by Eq. 1 with $x = r/R_{500}$, $x_c = 0.303$, $\alpha = 0.525$, and $\beta = 0.768$ (see Sect. 3) and we investigate β -models given by Eq. 1 with $\alpha = 0$, $\beta = 2/3$, and $x_c = 0.05, 0.1, 0.2, 0.3$, and 0.4 ($x_c = r_c/R_{500}$, where r_c is the usual β -model core radius).

For all models we compute luminosity profiles (spherically symmetric) which are then cylindrically integrated to obtain 'projected' luminosities as a function of cluster-centric distance. Finally these are normalised at R_{ap} where $L(< R_{\text{ap}}) = L_{\text{ap}}$ and shown in Fig. A.1 for $R_{\text{ap}} = 0.5 \times R_{500}$. The figure shows that, with respect to the AB-model, β -models with small core radii yield centrally concentrated luminosity profiles, which in turn are shallow at large radii. The opposite is true for β -models with large core radii, which predict very extended profiles. With respect to the AB-model, a β -model with $x_c = 0.05$ underestimates L_{500} by $\sim 20\%$ while for $x_c = 0.4$ it yields a factor of 2 larger value.

We investigate the effect of modeling on global luminosities by computing L_{500} and $L_{\text{tot}} = L(< 5 \times R_{500})$ as a function of R_{ap} . In Fig. A.2 we show the β -model to AB-model ratio of L/L_{ap} (the normalised luminosity profile) evaluated at R_{500} (i.e. $L = L_{500}$, solid lines) and $5 \times R_{500}$ (i.e. $L = L_{\text{tot}}$, dashed lines) as a function of R_{ap} . With respect to the AB-model, β -models with small/large core radii underestimate/overestimate L_{500} for apertures smaller than R_{500} , while for $R_{\text{ap}} > R_{500}$ this behavior is reversed. Total luminosities L_{tot} are always higher/lower than the AB-model estimates for β -models with small/large core radii and the difference increases with decreasing R_{ap} .